Research paper

Dry early Holocene revealed by sand dune accumulation chronology in Bayanbulak Basin (Xinjiang, NW China)

The Holocene
2014, Vol. 24(5) 614–626

DOI: 10.1177/0959683614523804
hol.sagepub.com
SAGE

Hao Long,[1,2] Ji Shen,[1] Sumiko Tsukamoto,[2] Jianhui Chen,[3] Linhai Yang[4] and Manfred Frechen[2]

Abstract

Understanding the Holocene climate changes (especially moisture variation) and their mechanisms in the semiarid–arid Central Asia (SCA) is very important, as water availability is crucial for sustainable developments in this area. This study presents chronostratigraphy of an aeolian sedimentary sequence from Bayanbulak Basin (Xinjiang, NW China), aiming to infer the Holocene moisture history in the SCA. Luminescence dating technique was selected to construct the age framework of the study section. Since the luminescence signal intensity of quartz from the samples was too low to be detected, feldspar was used as an alternative dosimeter. A newly developed post-infrared (IR) IR-stimulated luminescence (IRSL) (pIRIR) dating protocol on K-feldspar was applied to determine the ages of samples. A set of tests on luminescence characteristics was performed and demonstrate that this method is suitable and the resultant ages are reliable. Combined with the stratigraphic investigation on the sand dune/palaeosol section, the results imply a very dry climatic condition characterized by sand dune accumulation at ~9–8 kyr, and a wet interval of 5–1.6 kyr when a soil layer was formed. This moisture variation pattern is consistent with that inferred from many lacustrine records in the SCA, suggesting a widespread dry period at 11–8 kyr. The present results appear to challenge a new stalagmite $\delta^{18}O$ sequence, located nearby to Bayanbulak Basin, which instead suggested a humid early Holocene.

Keywords

Asian monsoon, Holocene moisture variation, luminescence dating, sand dune, semiarid–arid Central Asia, Westerlies

Received 19 September 2013; revised manuscript accepted 21 January 2014

Introduction

During the past two decades, a variety of palaeoenvironmental records have been reported to document the Holocene climate change (especially moisture variation) and the atmospheric circulation evolution in the mid-latitude Asian continent (e.g. reviews by An et al., 2000; Chen et al., 2008; Feng et al., 2006; Herzschuh, 2006; Wang et al., 2010). The mid-latitude Asian continent can be divided into two distinct climatic regions (Dando, 2005), that is, the humid eastern part of Asia (monsoonal Asia, mainly controlled by monsoon circulation) and the semiarid–arid Central Asia (SCA) in the western part, climatically dominated by the mid-latitude Westerlies (Figure 1a). Concerning the monsoonal Asia, the Asian monsoon variations and rainfall changes during the Holocene have apparently been well documented by a set of precisely dated records from cave (stalagmite) deposits, as well as marine, peat and lake sediments (Long et al., 2010, 2012c). Compared with the broad understanding of evolution and mechanisms of the palaeoclimate in monsoonal Asia, however, the past climate patterns during the Holocene in the SCA are poorly documented and understood. For instance, there are controversial points of view on the temporal patterns of effective moisture variations during the Holocene; especially, the early Holocene humidity conditions in this region (such as Xinjiang, NW China) is still a debatable topic (e.g. Chen et al., 2008; Li et al., 2011b). As a result, we still know little about its climate evolutionary patterns and forcing mechanisms. This lack of understanding is partly because of the complex interplay of competing forcing factors controlling regional climate; these factors include the low-latitude summer monsoonal circulation, the mid-latitude Westerlies (Chen et al., 2008) and orographic influences of the Tibetan Plateau (Broccoli and Manabe, 1992). Thus, for fully understanding the regional climate change in the SCA and its causes, more records with clear climatic implications and reliable age control are necessary.

It should be noted that the majority of the records on the Holocene moisture variation from the SCA are based on lake sedimentary sequences. For these lake records, there are potential problems in ^{14}C dating–based chronology (Hou et al., 2012; Long et al., 2011; Mischke et al., 2013) and climatic proxy interpretation (Long et al., 2012c), which may cause different climatic

[1]Nanjing Institute of Geography and Limnology, Chinese Academy of Sciences (NIGLAS), China
[2]Leibniz Institute for Applied Geophysics (LIAG), Germany
[3]MOE Key Laboratory of Western China's Environmental System, Lanzhou University, China
[4]Cold and Arid Regions Environmental and Engineering Research Institute, Chinese Academy of Sciences, China

Corresponding author:
Hao Long, State Key Laboratory of Lake Sciences and Environment, Nanjing Institute of Geography and Limnology, Chinese Academy of Sciences (NIGLAS), 210008 Nanjing, China.
Email: longhao@niglas.ac.cn; lzugeolh@gmail.com

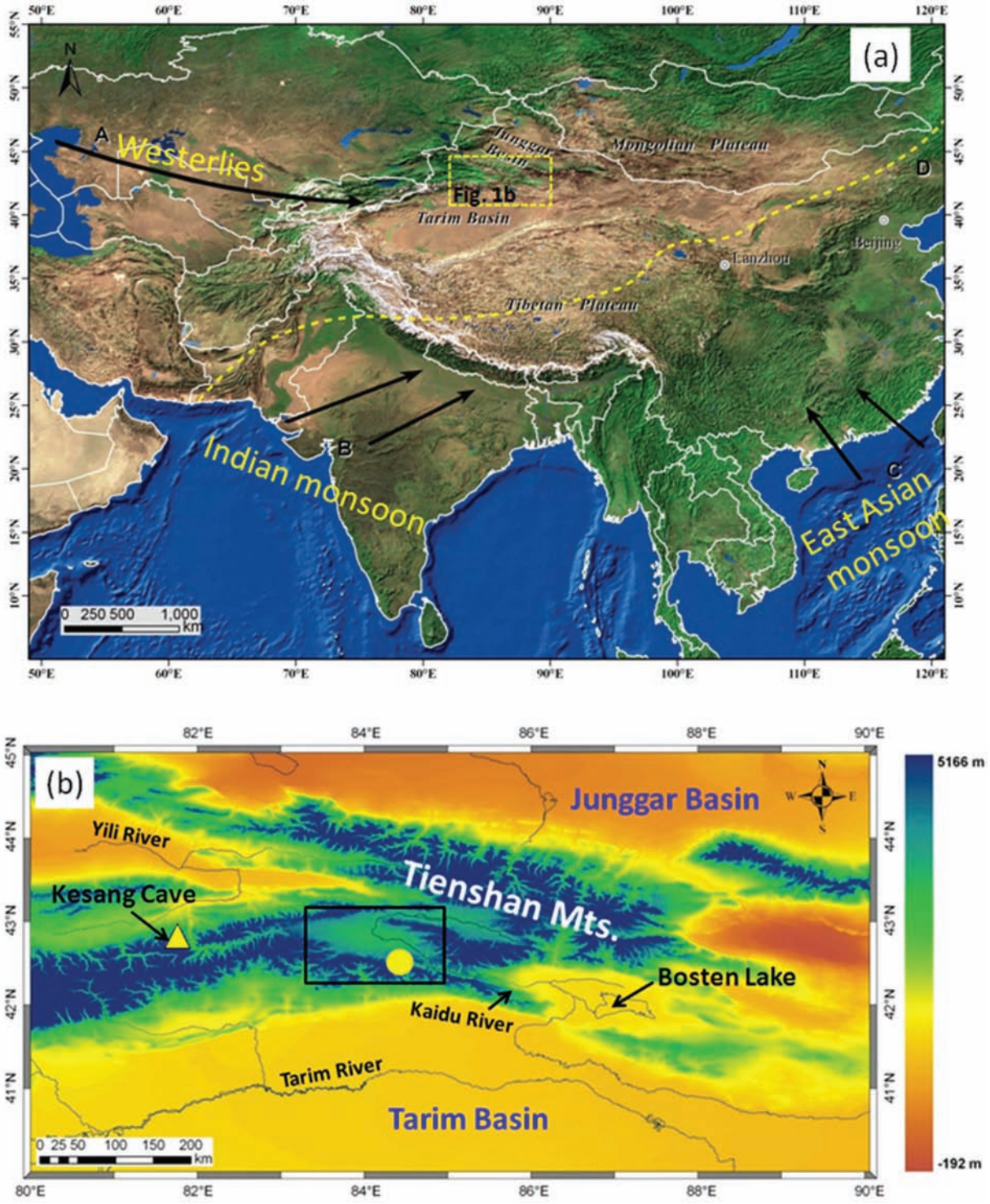

Figure 1. (a) Map showing the location of the study area (denoted by the yellow dashed rectangle), and the dominant circulation systems (arrows) including Westerlies (A), Indian monsoon (B) and East Asian monsoon (C). The modern Asian summer monsoon limit (Chen et al., 2008) is denoted by a dashed line (D). (b) Topographic map of Tien Shan Mountains, and the location of Bayanbulak intermontane basin, as shown in the rectangle. Filled circle denotes location of the dune field from the southeastern edge of Bayanbulak basin. The filled triangle shows the location of Kesang Cave.

inferences even in same study site. For lake sediments from these areas, organic matter content is always extremely low, and thus, bulk organic matter is normally used for ^{14}C dating, but this material often suffers from contamination from sources of 'old carbon' (hard water reservoir effect), varying from several hundreds to thousands of years in different lakes (Long et al., 2011). Even in one lake, the reservoir effects varied through time, as shown by our recent work (Long et al., 2012a), but the previous studies mostly assumed a constant ^{14}C reservoir effect over sediments burial time. Therefore, the uncertainties of ^{14}C-based dating in many of the previous records could make it difficult to precisely constrain the timing of lake levels and corresponding regional moisture history.

Besides lacustrine sediments, sand dune sediments from arid and semiarid areas can also be considered as an archive of past moisture variation and the inclusive aeolian sand/palaeosol stratigraphy is clearly indicative of regional aridity/wetness conditions. In addition, with the advances in luminescence dating methods, which can directly date periods of sand deposition, it has become possible to provide more precise correlations of

periods of dune evolution to other palaeoclimatic proxies and records (Singhvi and Porat, 2008). Alternating moisture conditions in the late Quaternary have been reconstructed in sand dune sediments from the arid and semiarid areas all over the world, for example, in North America (Forman et al., 2005; Goble et al., 2004; Mason et al., 2004; Miao et al., 2007), Northern China (Long et al., 2012b; Lu et al., 2005; Mason et al., 2009; Yang et al., 2013) and Africa (Bristow et al., 2007; Telfer and Thomas, 2007; Thomas and Burrough, 2012). Sand dunes or stabilized dune fields, which are independent of the lake sedimentary records used in most previous studies in the SCA, as alternative robust geomorphological archive recording past climate conditions, could thus provide a valuable source of information on the temporal and spatial moisture changes during the late Quaternary (Lancaster, 2008; Thomas and Burrough, 2012). Although sand dunes or stabilized dune fields cover large area in the SCA, few sand dune records have been reported for constructing past moisture changes during the late Quaternary in this region (Li and Fan, 2011). Here, we report, for the first time, the chronostratigraphy of an aeolian sedimentary sequence from Bayanbulak Basin (Xinjiang, NW China), in order to reconstruct the Holocene moisture history in the SCA.

Study area and research materials

Bayanbulak Basin (42°42′–43°12′N, 83°15′–84°45′E) is one of intermontane basins in the Tien Shan Mountains which is 2500 km long, up to 7400 m high, extending through Western China, Kazakhstan and Kyrgyzstan (Figure 1b). This basin, ~150 km long from east to west and ~50-km wide from south to north, is a wide endorheic sedimentary basin filled by large alluvial fans. The base level of the basin is at an altitude of about 2400 m, while the fans reach altitudes of about 3000 m all around the basin. Kaidu River meanders through the basin, resulting in swamp plains in the middle of Bayanbulak Basin. The annual average temperature is −4.7°C, and annual mean precipitation and evaporation are 276 and 1035 mm in the basin, respectively. At present, winds are dominated by the Westerlies or northwest wind in this region. The landscape of Bayanbulak region is vegetated dominantly by subalpine, alpine meadow and steppe, as well as swamp and swamp-meadow in the middle of the basin.

In the southeastern edge of Bayanbulak Basin, two areas (~50 km^2 for each) with sand dune landforms were found during our field investigation in 2011. These dune landforms are also feasible to be identified from aerial photographs. In the dune field, the sand dune bodies are mostly covered by palaeosol and are well vegetated (Figure 2a), and using reconnaissance across the dune field, we also found several eroded sites where palaeosol/sand dune sediments are exposed (Figure 2b). A series of sites distributed in the whole dune field, where ~2-m-thick sediments' exposure because of erosion provided us with the opportunity to observe both vertical and horizontal sediment variation. They show overall consistent stratum structures for these dune crests. In this study, one site, Tianehu1 (TEH1) from a crest of dune landform (Figure 2b) in the western dune field was selected for detailed investigations. The section was excavated down to the dune sand layer (Figure 3a).

The section TEH1 is 305 cm thick and can be divided into six stratigraphic units from bottom to top based on bedding, colour and texture (see the section picture in Figure 3a). The lowermost unit (U1: 305–247 cm) consists of well-sorted light-coloured sands and has a typical aeolian dune structure with distinct cross-bedded sand layers, suggesting a dune formation period; the overlying unit (U2: 247–226 cm) mainly consists of yellowish consolidated silty sand, indicative of strengthening pedogenic process and transition from dune sands to palaeosol (Figure 3b); this transitional layer is covered by a typical palaeosol unit (U3: 226–170 cm) composed of darkish clayish silts (or silty loam), showing the strongest pedogenic intensity in the entire sequence; further to the top, another palaeosol layer (U4: 170–90 cm) is mainly composed of grey sandy silts and alternated by fine to medium silts with centimetre-scale horizontal and subhorizontal bedding, representing relatively weak pedogenesis; the Unit U5 (90–30 cm) consists of sandy loess sediments and the uppermost unit (U6: 30–0 cm) is the modern vegetated surface soil. To summarize, the lower part (including units U1, U2 and U3) of this section is characterized by the A/B/C profile (Figure 3b).

In order to construct the chronological framework of section TEH1, 10 samples were obtained for luminescence dating by hammering steel cylinders (5 cm diameter and 20 cm long) into the freshly cleaned profile wall with careful consideration of the changes in sedimentary units. The filled cylinder was removed from the sediments; the exposed ends were capped and then sealed with aluminium foil for transport to laboratory.

Luminescence dating method

Sample preparation and equipments

In the laboratory, the sediments at each end of the cylinders were scraped off, and the material from the middle part of the cylinder, not exposed to light, was used for equivalent dose (D_e) measurement. The sediment for D_e measurements were first wet sieved to obtain the coarse grain (CG) fraction (150–200 μm), and then treated with 10% HCl and 30% H_2O_2 to remove any carbonates and organic matter. In general, quartz mineral is predominantly used for luminescence dating. It was thus initially intended to use CG quartz for dating the sediments for this study. The CG fraction were treated by heavy liquid density separation with sodium polytungstate to separate the quartz from any heavy minerals (>2.70 g/cm^3) and feldspars (<2.62 g/cm^3). The quartz grains were etched with 40% HF for 60 min (followed by an HCl rinse) to remove the outer alpha-irradiated layer of the quartz grains and also to eliminate any potential feldspar contamination. Unfortunately, the quartz optically stimulated luminescence (OSL) signal intensity was too low (Figure 4a), suggesting that OSL dating may be impractical for routine use. Therefore, feldspar was used as an alternative dosimeter because of its bright luminescence signal. Using the same density separation method, the K-rich feldspars (<2.58 g/cm^3) were separated from the Na-rich feldspars (>2.58 g/cm^3). Considering that HF etching on feldspar tends to cause deep pitting and to preferentially attack the cleavage planes of the feldspar grains rather than removing a uniform shell from the grains as assumed (Duller, 1994) the K-rich feldspar separates were not treated with HF.

D_e was measured on an automated luminescence reader (Risø TL/OSL DA-15) equipped with a $^{90}Sr/^{90}Y$ beta source. For the quartz OSL, blue LEDs (470 nm) were used for stimulating the aliquots, and a 7.5 mm Hoya U-340 filter was used as signal detection filter in front of the photomultiplier tube. For K-feldspar luminescence measurement, infrared (IR) LEDs (870 nm) were used, and the IR-stimulated luminescence (IRSL) signal of K-feldspar minerals was detected through a combination of Schott BG-39 and Corning 7-59 filters in the blue light spectrum between 320 and 450 nm.

Measurement protocol for D_e estimation

The single greatest factor which has prevented the widespread uptake of luminescence dating using feldspars is the phenomenon of anomalous fading (Wintle, 1973). Recently, advances have been achieved in isolating a luminescence signal from feldspar which is less affected by anomalous fading. Thomsen et al. (2008) first reported that the IRSL signal observed at an elevated temperature following a prior IR stimulation at 50°C (i.e. post-IR IRSL signal, abbreviated pIRIR) is more stable and has a much

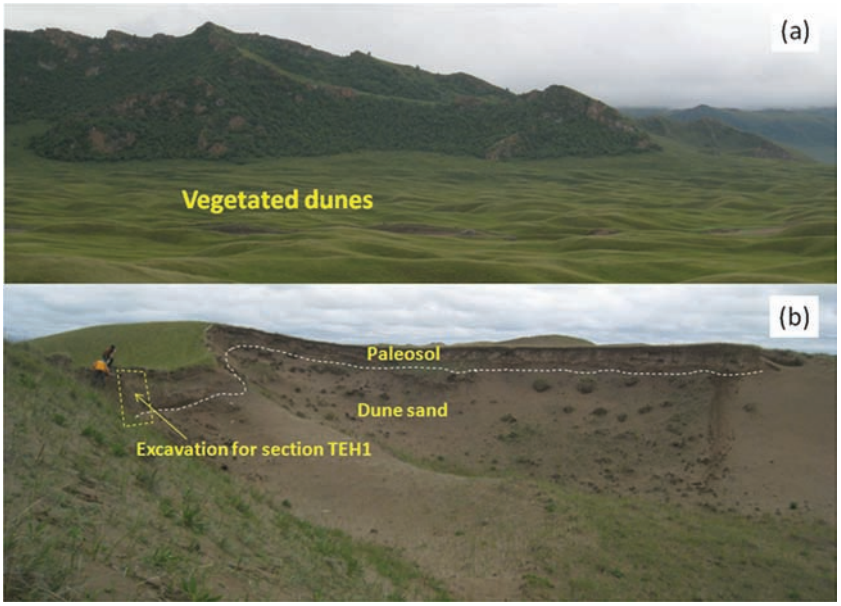

Figure 2. Field photographs showing (a) the vegetated dune landscapes and (b) exposed sand dune sediments because of erosion.

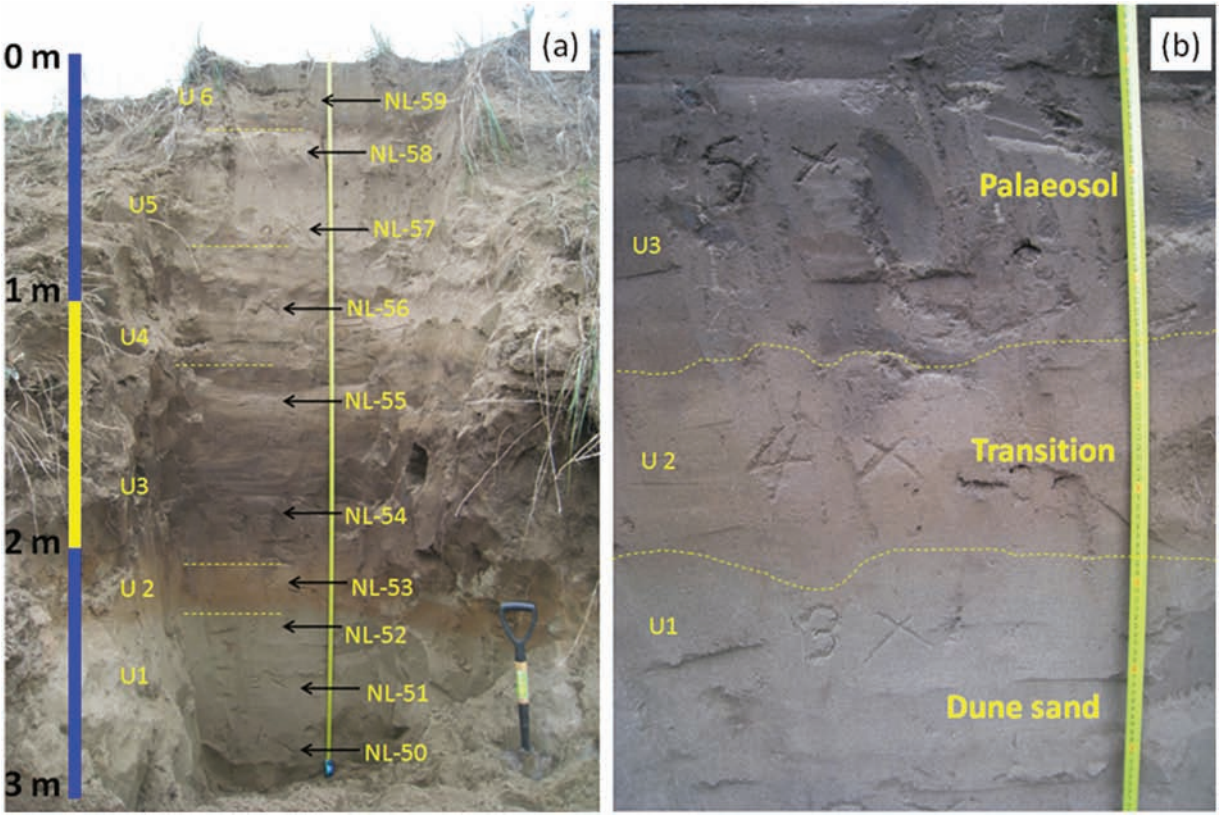

Figure 3. (a) Photograph showing the stratigraphy of the study section (TEH1) and (b) close view on three stratigraphic units (U1, U2 and U3).
TEH1: Tianehu1.

lower fading rate than the conventional IRSL signal measured at 50°C (abbreviated $IRSL_{50}$) for the same CG K-feldspar sample. Recently, Madsen et al. (2011) and Reimann et al. (2011) modified and applied this protocol for dating K-feldspar of coastal sands of Holocene age using lower preheat and pIRIR stimulation temperatures, which was confirmed by independent age control. The pIRIR single aliquot regenerative dose (SAR) protocol used for this study is based on the one proposed by Reimann and Tsukamoto (2012), to measure a standard IRSL signal at 50°C ($IRSL_{50}$), as well as an IR signal at an elevated temperature (at 150°C, $pIRIR_{150}$) after an $IRSL_{50}$. For both $pIRIR_{150}$ and $IRSL_{50}$ signals, the integrated signal was calculated from the first 10 s minus a background from the last 10 s.

Dose rate determination

The material for determining dose rate was first dried and homogenized. The radionuclide concentrations (U, Th and K content) of

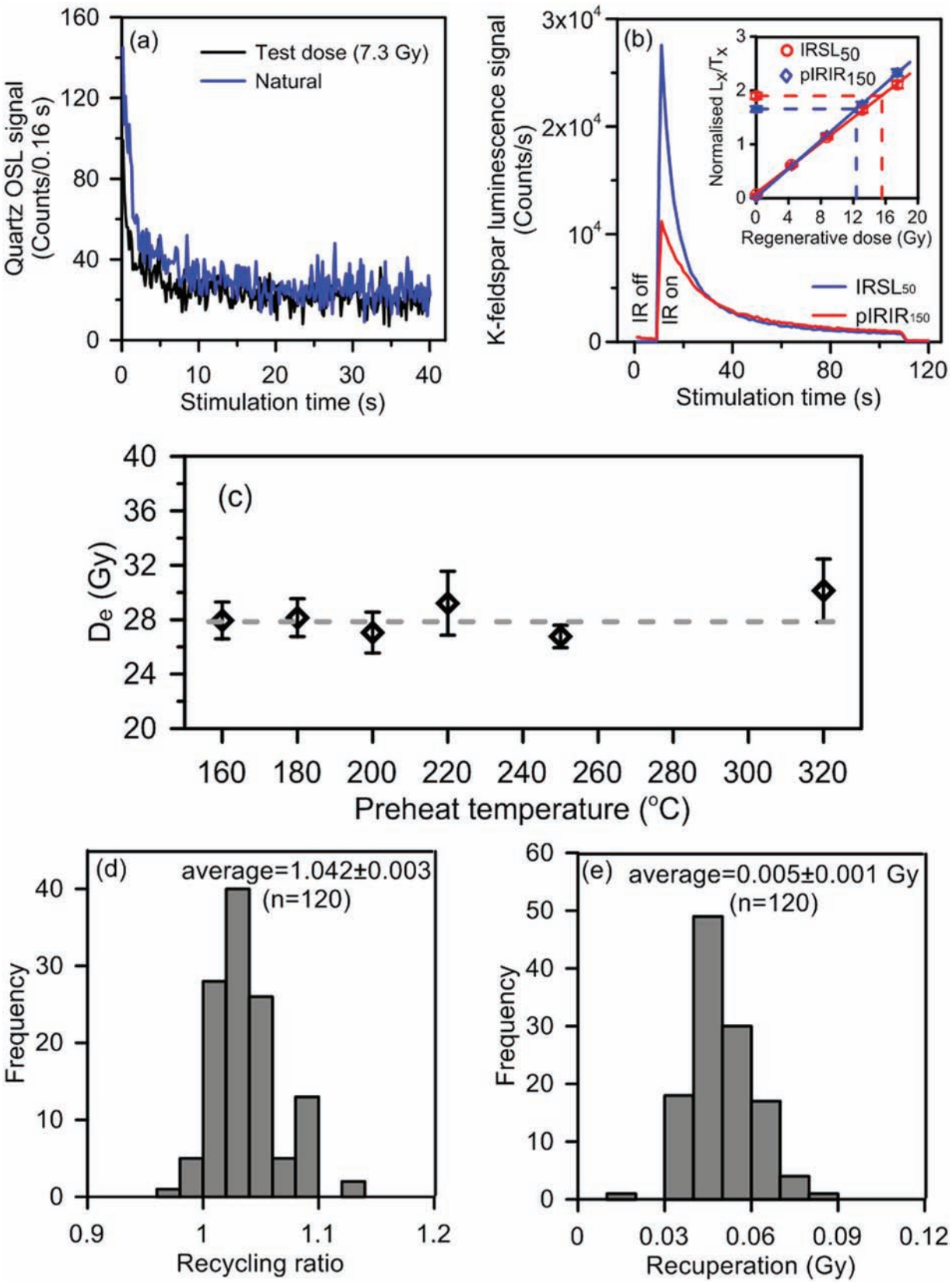

Figure 4. (a) An example showing very low quartz OSL signals, (b) typical $IRSL_{50}$ and $pIRIR_{150}$ decay curves for K-feldspar and corresponding growth curves (inset) from a representative sample (NL-54), (c) $pIRIR_{150}$ equivalent doses determined for sample NL-50 using different measurement conditions, (d) histograms summarizing the recycling ratios, and (e) recuperation values for $pIRIR_{150}$ measurements.
OSL: optically stimulated luminescence; $IRSL_{50}$: infrared-stimulated luminescence signal measured at 50°C; $pIRIR_{150}$: post-IR IRSL signal at 150°C.

the surrounding sediment were measured by neutron activation analysis (NAA) method, to obtain the external dose rate on K-feldspar. The conversion factors of Guérin et al. (2011) and the β-attenuation factors after Mejdahl (1979) are used to calculate the external β- and γ-dose rates. The 'in situ' water content of the samples is measured to correct the α-, β- and γ-dose rates for the water attenuation (Aitken, 1985). According to Prescott and Hutton (1994), the cosmic dose rate is calculated as function of the altitude and latitude of the sampling sites, the burial depth and the density of the overburden. Additionally, the external α-dose

rate for alpha-irradiated outer rim of the K-feldspar grains and the internal dose rate have to be considered for K-feldspar age calculation. An α-value of 0.15 ± 0.05 is used according to Balescu and Lamothe (1994) for external α-dose rate calculation of the outer 0.25 mm (following Aitken, 1998) of the feldspar grains. For the internal β-dose rate, a K concentration of 12.5 ± 0.5% (Huntley and Baril, 1997) and a Rb content of 400 µg/g (following Huntley and Hancock, 2001) are assumed. Finally, the total dose rates were calculated using the conversion factors of Guérin et al. (2011).

Dating results

Luminescence characteristics

Figure 4a shows decay curves from a representative sample (NL-50), suggesting very low OSL signals. Similarly, all other nine CG quartz samples showed very dim natural and regenerated OSL signals, even for large (8 mm) aliquots. Only several tens of counts for the first 0.16 s stimulation were obtained when a test dose of ~7.3 Gy was applied. Thus, the quartz mineral is considered to be unsuitable for luminescence dating in the current case. Subsequently, we focused on the IRSL signal of K-feldspar for dating. In Figure 4b, an example of natural $IRSL_{50}$ decay curve and the immediately following $pIRIR_{150}$ decay curve for one aliquot of sample NL-54 is shown, together with the dose response curves of both the signals for the same aliquot.

In order to check the suitability of the measurement protocol used for D_e determination, we first tested the effect of different elevated-temperature pIRIR measurement conditions on D_e. A total of 18 aliquots of sample NL-50 were prepared for measurement under six different temperature conditions (three for each condition). Preheat temperatures of 160, 180, 200, 220, 250 and 320°C were applied, followed by an IR stimulation at 50°C, and then a second IR stimulation at an elevated temperature 30°C lower than the preheat temperature was applied, except for the 250°C preheat where a pIRIR stimulation at 225°C was used (Figure 4c). There seems to be no clear trend in the D_e value obtained regardless of the preheat temperature used prior to this IR_{50} measurement. Because of the negligible residual doses (see following) derived from measurements at preheat of 180°C, we chose a pIRIR stimulation at 150°C for D_e measurement.

The recycling ratio, recuperation and dose-recovery tests for the $pIRIR_{150}$ SAR protocol were examined for all samples. Figure 4d summarizes the recycling ratios for the $pIRIR_{150}$ signal; the overall recycling ratio for all samples is 1.042 ± 0.003 (n = 120), illustrating that the sensitivity correction worked well and the measurement following laboratory irradiations is reproducible. Figure 4e summarizes the recuperation values, that is, the response to a zero-Gy laboratory dose, measured just after the SAR cycle for natural dose; recuperation is in general less than 0.09 Gy (n = 120) and is considered acceptably small.

Furthermore, dose-recovery tests were carried out for the 10 samples (three aliquots for each sample). First, the aliquots were bleached for 4 h under a solar simulator lamp (Hönle SOL2). They were then given a known dose of ~26.1 Gy. All aliquots were then measured using the $pIRIR_{150}$ protocol. Data of dose-recovery test for all 10 samples (30 discs in total) are presented in Figure 5a. Most measured-to-given dose ratios for $pIRIR_{150}$ signals range from 0.9 to 1.1 after subtracting the residual dose values. The mean dose-recovery ratio is 0.982 ± 0.007, suggesting that our protocol is able to accurately measure doses given in the laboratory before heating and optical treatment. All these laboratory tests indicate that the overall behaviour of the SAR protocol when applied to the pIRIR signals from the samples appears to be satisfactory.

It is known that feldspar luminescence is bleached by daylight more slowly than the OSL from quartz (Buylaert et al., 2012; Godfrey-Smith et al., 1988; Thomsen et al., 2008) and that elevated-temperature IRSL bleaches more slowly than IRSL stimulated at low temperatures (Reimann and Tsukamoto, 2012). To examine the bleachability of the $pIRIR_{150}$ signal of our samples, which is of particular importance in luminescence dating of young samples, we measured the residual doses after bleaching in a solar simulator. For all discs (3 for each of 10 samples) exposed in the Hönle SOL2 for 4 h, the tests showed residual doses ranging from −0.09 to 0.2 Gy (Figure 5b), resulting in possible age errors of approximately 50 years for the studied sediments. These obtained residual doses are much less than that of pIRIR signal measured at much higher temperatures ($pIRIR_{225}$ and $pIRIR_{290}$), which have been used more commonly (e.g. Buylaert et al., 2009; Thiel et al., 2011). Considering the residual dose is negligible compared with the D_e values of the Holocene sediments, the residual doses were not subtracted from the measured D_e values for age calculation.

Anomalous fading

Anomalous fading rate of feldspar luminescence signal is usually quantified by the g-value to represent the luminescence signal loss per decade of normalized storage time (Huntley and Lamothe, 2001). The fading is ubiquitous for most of feldspars when the IRSL signal is measured at low temperature (e.g. 50°C, Huntley and Lamothe, 2001). In contrast, pIRIR signal could be used to minimize fading rate to a negligible level (e.g. Reimann and Tsukamoto, 2012). To confirm this, six aliquots for each sample were measured to determine g-values for both $IRSL_{50}$ and the $pIRIR_{150}$ signals using the method described by Auclair et al. (2003). The g-value of each aliquot was obtained by fitting a linear regression line to the sensitivity-corrected IRSL and pIRIR signals as a function of logarithmic normalized storage time (Figure 5c). It shows a pronounced difference in the slopes of the fitted linear function between the two feldspar signals, which is equivalent to the g-value. We obtained laboratory-fading rates for all samples for both signals, which are summarized as histograms in Figure 5d. The mean $pIRIR_{150}$ g-value is 1.23 ± 0.09%/decade (n = 60), and the mean $IRSL_{50}$ g-value is 5.26 ± 0.13%/decade (n = 60). It is obvious that the g-values for the $pIRIR_{150}$ signal are significantly lower compared with that derived from the $IRSL_{50}$ signal. We calculated the average g-value from six aliquots and its standard error for each sample (Table 1).

Although g-values of the $pIRIR_{150}$ signal apparently suggest anomalous fading in a certain degree, we did not correct the $pIRIR_{150}$ ages for anomalous fading. This is because the laboratory-fading experiments should not be considered as convincing evidence for loss of trapped charge during storage, especially for such low fading rates of 1.0–1.5%/decade. Most likely, these low apparent fading rates are an artefact of our measurement procedure, for instance, because of inaccurate sensitivity correction after storage (Buylaert et al., 2012). Although IRSL ages have successfully made use of a fading rate correction (Buylaert et al., 2011; Huntley and Lamothe, 2001), some studies have suggested that corrections based on laboratory-fading rates do not provide accurate age estimates (Li et al., 2008, 2011a; Reimann et al., 2011; Wallinga et al., 2007). Furthermore, even normal quartz samples could give a mean g-value of ~1.0%/decade (similar to the values for our $pIRIR_{150}$ signal; Buylaert et al., 2012), which would predict age underestimates of ~10% or more. If the $pIRIR_{150}$ signal is unstable on a laboratory time scale, it must be similar to that of the quartz OSL signal, which is widely accepted as a stable signal. Thus, our data give evidence that the use of the $pIRIR_{150}$ signal is able to reduce anomalous fading even to a negligible level, and so the equivalent doses derived from the uncorrected $pIRIR_{150}$ signal were used for luminescence age calculation.

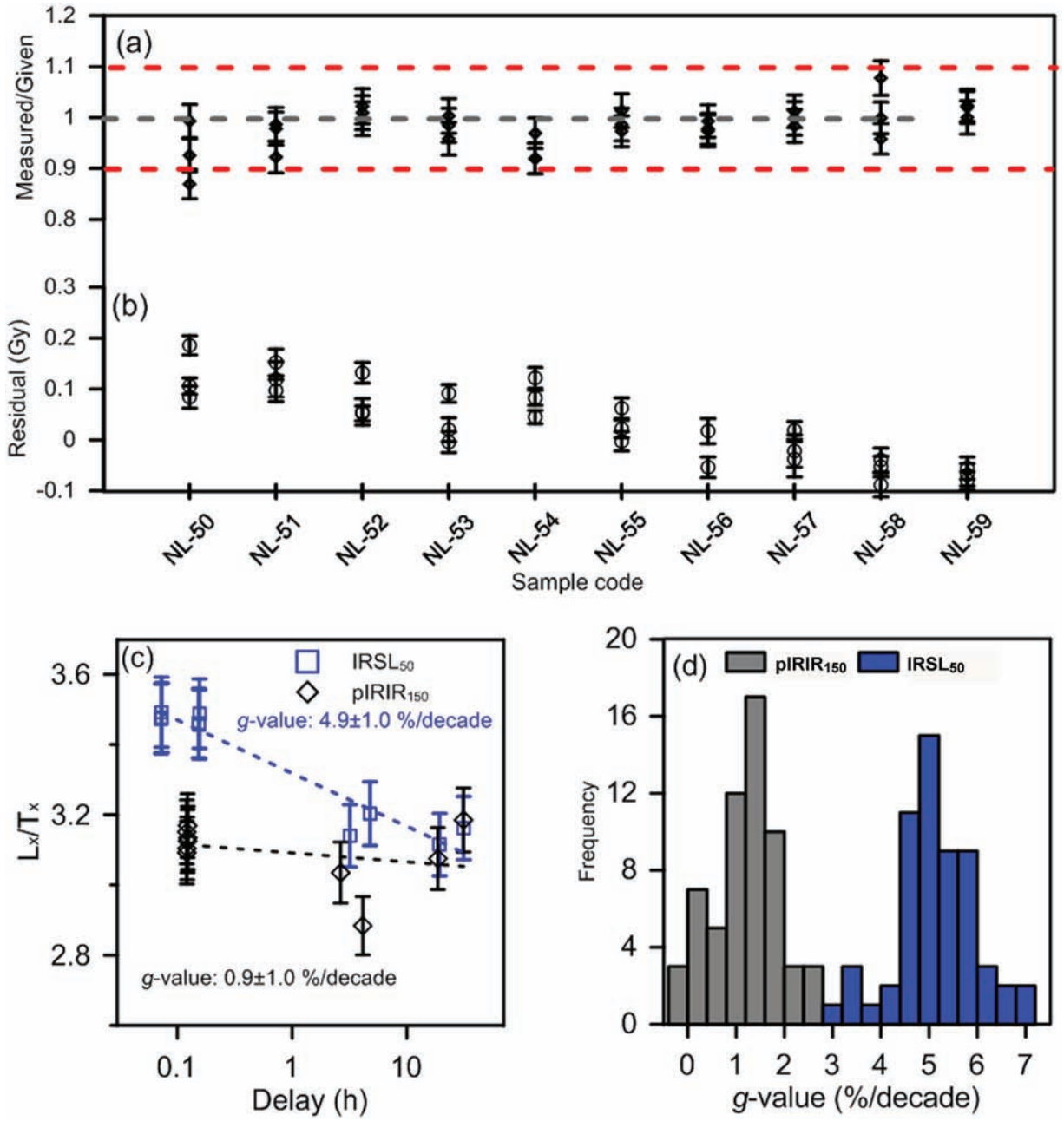

Figure 5. (a) Dose-recovery tests and (b) residual tests on $pIRIR_{150}$ signal for the 10 samples (three discs were used for every test for each sample). (c) Fading rate (*g*-value) determination of $IRSL_{50}$ and $pIRIR_{150}$ signals from a representative aliquot of sample NL-50. (d) Histogram summarizing $IRSL_{50}$ and $pIRIR_{150}$ fading rates for all 10 samples (six aliquots for each sample).
$IRSL_{50}$: infrared-stimulated luminescence signal measured at 50°C; $pIRIR_{150}$: post-infrared infrared-stimulated luminescence signal at 150°C.

Dose rates, equivalent doses and ages

The results of dose rate calculation are listed in Table 1, suggesting that the total dose rate (3.2–3.6 Gy/kyr) varies little among different samples for the entire profile. This indicates homogeneous natural irradiation from the surrounding sediments to the K-feldspar minerals at the study site. For each sample, 12 aliquots were used for the D_e measurement derived from $pIRIR_{150}$ signal with small aliquots (2 mm) each containing about 50–100 individual grains (Duller, 2008). All D_e estimates for the 10 samples are summarized in Table 1. Partial bleaching, the incomplete resetting of the luminescence signal owing to inadequate exposure to daylight before deposition, might be a potential problem in using IRSL signals for sediment dating (Reimann et al., 2011). The resulting D_e distributions for all samples from section TEH1 are shown in Figure 6. All distributions are generally narrow with small (<20%) overdispersion values (see Table 1), which were calculated using the central age model (CAM; Galbraith et al., 1999). But for the youngest sample (NL-59) from the uppermost layer (nearly surface), the overdispersion value was as high as 34%, showing a relatively broad distribution of D_e. This is likely to be because of a poor signal-to-noise ratio for such a young sample, instead of partial bleaching. As a result, we believe that the $pIRIR_{150}$ signals of all studied samples were generally well bleached before deposition. Therefore, the CAM D_e values were used for age calculation, and the uncertainty given is the standard error. According to the CAM D_e and total dose rate, ages were calculated for all samples (Table 1).

Following the applied quality tests above, we conclude that the $pIRIR_{150}$ protocol is suitable for the determination of D_e for our K-feldspar samples. The D_e distributions indicate complete bleaching of the $pIRIR_{150}$ signal. The near-surface sample (NL-59) was dated to ~0.1 kyr, which is close to a modern age and gives further evidence for sufficient bleaching of our samples prior to deposition. All of the 10 samples are in good stratigraphic order, giving us confidence in the dating results.

Table 1. Luminescence dating data for the 10 samples.

Stratigraphic units		U1			U2	U3		U4	U5		U6
Sample ID		NL-50	NL-51	NL-52	NL-53	NL-54	NL-55	NL-56	NL-57	NL-58	NL-59
Depth (cm)		305	280	250	235	210	160	120	88	52	25
H_2O (%)		1.6 ± 5	1.7 ± 5	3.0 ± 5	14.3 ± 5	29.0 ± 5	18.9 ± 5	4.4 ± 5	2.9 ± 5	2.9 ± 5	4.9 ± 5
Cosmic dose (Gy/kyr)		0.19 ± 0.01	0.20 ± 0.02	0.21 ± 0.02	0.22 ± 0.02	0.23 ± 0.02	0.25 ± 0.02	0.27 ± 0.02	0.28 ± 0.02	0.30 ± 0.03	0.31 ± 0.03
U (ppm)		1.35 ± 0.07	1.31 ± 0.07	1.4 ± 0.07	1.91 ± 0.08	2.00 ± 0.08	1.83 ± 0.08	1.35 ± 0.07	1.15 ± 0.06	1.43 ± 0.07	1.42 ± 0.07
Th (ppm)		5.50 ± 0.19	5.14 ± 0.18	6.14 ± 0.21	8.31 ± 0.27	9.71 ± 0.29	11.9 ± 0.35	6.93 ± 0.24	5.20 ± 0.18	5.85 ± 0.20	5.62 ± 0.20
K (%)		1.92 ± 0.06	1.96 ± 0.06	1.90 ± 0.06	2.01 ± 0.06	2.03 ± 0.06	1.98 ± 0.06	2.00 ± 0.06	1.90 ± 0.06	1.97 ± 0.06	1.75 ± 0.06
Alpha dose rate (Gy/kyr)		0.12 ± 0.08	0.11 ± 0.08	0.13 ± 0.08	0.15 ± 0.07	0.14 ± 0.05	0.17 ± 0.07	0.13 ± 0.08	0.11 ± 0.08	0.12 ± 0.08	0.12 ± 0.07
External dose rate (Gy/kyr)		2.76 ± 0.13	2.77 ± 0.13	2.77 ± 0.13	2.81 ± 0.11	2.58 ± 0.09	2.89 ± 0.10	2.92 ± 0.12	2.72 ± 0.13	2.91 ± 0.13	2.65 ± 0.12
Internal dose rate (Gy/kyr)		0.69 ± 0.09	0.69 ± 0.09	0.69 ± 0.09	0.69 ± 0.09	0.69 ± 0.09	0.69 ± 0.09	0.69 ± 0.09	0.69 ± 0.09	0.69 ± 0.09	0.69 ± 0.09
Total dose rate (Gy/kyr)		3.45 ± 0.15	3.46 ± 0.15	3.46 ± 0.15	3.50 ± 0.14	3.27 ± 0.12	3.58 ± 0.13	3.61 ± 0.15	3.41 ± 0.15	3.60 ± 0.15	3.34 ± 0.15
$IRSL_{50}$	g-value (%/decade)	4.9 ± 1.0	5.3 ± 1.0	4.4 ± 1.1	5.2 ± 1.0	5.9 ± 1.0	6.1 ± 1.0	5.6 ± 1.0	5.0 ± 1.0	4.5 ± 1.0	5.8 ± 1.0
	Mean D_e (Gy)	24.49 ± 0.52	23.40 ± 0.5	23.29 ± 0.43	21.07 ± 0.63	12.35 ± 0.33	5.26 ± 0.10	4.39 ± 0.11	2.94 ± 0.04	1.78 ± 0.04	0.31 ± 0.01
	Age (kyr)	7.10 ± 0.36	6.76 ± 0.34	6.73 ± 0.33	6.02 ± 0.30	3.77 ± 0.18	1.47 ± 0.06	1.22 ± 0.06	0.86 ± 0.04	0.49 ± 0.02	0.09 ± 0.01
$pIRIR_{150}$	g-value (%/decade)	1.3 ± 1.1	1.6 ± 1.0	0.5 ± 1.1	1.1 ± 1.0	1.9 ± 1.1	1.8 ± 1.0	1.3 ± 1.0	0.9 ± 0.9	0.3 ± 0.9	1.6 ± 1.0
	Mean D_e (Gy)	29.5 ± 1.6	28.6 ± 1.3	28.6 ± 1.2	26.1 ± 0.7	15.1 ± 1.5	6.3 ± 0.5	5.3 ± 0.6	4.1 ± 0.7	2.3 ± 0.3	0.5 ± 0.02
	CAM D_e (Gy)	29.4 ± 0.5	28.4 ± 0.3	28.4 ± 0.4	25.9 ± 0.6	15.0 ± 0.5	6.1 ± 0.1	5.2 ± 0.2	4.0 ± 0.2	2.2 ± 0.1	0.4 ± 0.0
	Overdispersion (%)	4.6	3.3	3.5	8.2	10.1	7.6	10.9	14.8	12.5	33.9
	Age (kyr)	8.5 ± 0.4	8.2 ± 0.4	8.2 ± 0.4	7.4 ± 0.4	4.6 ± 0.2	1.7 ± 0.1	1.5 ± 0.1	1.2 ± 0.1	0.6 ± 0.0	0.1 ± 0.0

$IRSL_{50}$: infrared-stimulated luminescence signal measured at 50°C; $pIRIR_{150}$: post-infrared infrared-stimulated luminescence signal at 150°C; CAM: central age model.

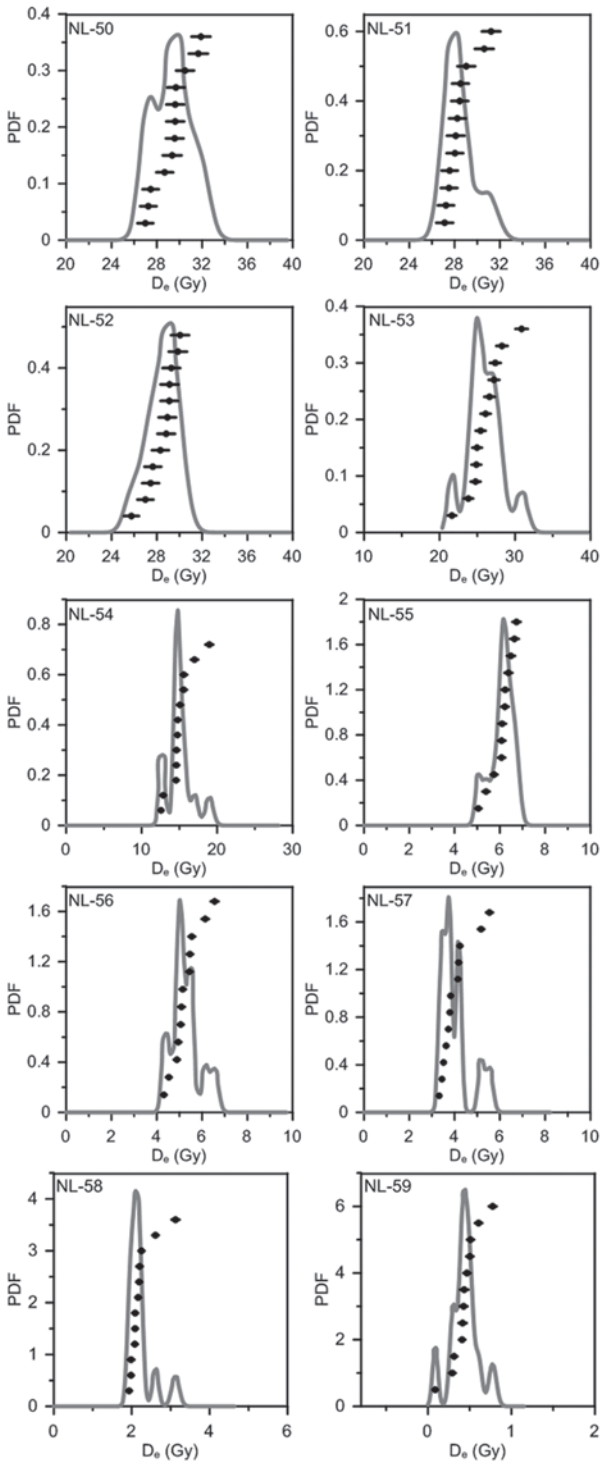

Figure 6. D_e distributions of the 10 samples.

Discussion

Chronostratigraphy of section TEH1 and palaeoclimatic implication

Luminescence dating methods directly determine the time elapsed since deposition of aeolian sand, and thus the timing of sand dune accumulation. However, the interpretation of luminescence ages from buried soils overlying dune sands seems more complex, because ages may record a combination of any of the following: (1) light exposure during soil parent material deposition (i.e. dune accumulation activity), (2) light exposure through bioturbation (potentially recording the time of dune stabilization and soil formation) and (3) light exposure of minor increments of sand deposited intermittently during pedogenesis (most likely for thick cumulative soils; Goble et al., 2004; Lu et al., 2011; Mason et al., 2009; Yang et al., 2012). In the current case, the two ages (4.6 ± 0.2 and 1.7 ± 0.1 kyr) from buried soil unit (U3) are thousands of years younger than ages (8.5 ± 0.4, 8.2 ± 0.4 and 8.2 ± 0.4 and 7.4 ± 0.4 kyr) of the underlying units (U1 and U2). And field observation did not show clear evidence for bioturbation in our profile. These considerations imply that luminescence ages from palaeosol layer can represent the timing of its formation under study at the section TEH1.

According to our field observation on the diagnostic sedimentary bedding, colour, texture and consistency (see the description in the section 'Study area and research materials' and Figure 7a), together with luminescence dating results, the chronostratigraphy of the profile TEH1 is shown in Figure 7b. The basal aeolian sand unit (U1) yields three ages (8.5 ± 0.4, 8.2 ± 0.4 and 8.2 ± 0.4 kyr); these ages are generally consistent within uncertainties, indicating a rapid sand dune accumulation before ~9–8 kyr. U2 was dated to 7.4 ± 0.4 kyr, and thus gives evidence for the onset of soil formation during a period of decreased sand dune mobility after the dune formation. U3 is a buried loam layer for which two ages (4.6 ± 0.2 and 1.7 ± 0.1 kyr) were obtained; this implies that the strongest pedogenesis occurred between ~4.6 and 1.7 kyr. Only one age of U4 (1.5 ± 0.2 kyr) suggests a relatively weak pedogenic process at around 1.5 kyr. Afterwards, loess layer (U5) formed from 1.2 ± 0.1 to 0.6 ± 0.0 kyr. The surface soil layer was dated to 0.1 ± 0.0 kyr.

Dune sands and palaeosol record regional variations in dune mobility and soil formation, and these are often linked to climate change (Lu et al., 2005, 2010; Mason et al., 2009). In general, aeolian dune sand indicates active sand transport with limited vegetation cover and decreased moisture, whereas a palaeosol represents wetter conditions with much less aeolian activity. The buried soils have greater silt and clay content than aeolian sand, indicating surface stability and vegetation cover. These interpretations have been broadly used in the palaeoenvironmental implications of dune mobility and stability in arid and semiarid regions over Northern China (e.g. Mason et al., 2009; Lu et al., 2010, 2011; Yang et al., 2012, 2013), although changing wind strength might also have played a role in sand dune evolution (e.g. Chase, 2009; Chase and Thomas, 2007; Long et al., 2012b). For this study, the chronostratigraphical investigation on the study profile can be used to construct an alternative history of dune sand accumulation and palaeosol formation, and thus variability of regional effective moisture.

Only one site (i.e. TEH1) might not be sufficient to figure out the complete moisture history during the past in the study area, but our survey across the whole dune field suggested overall consistent stratum structures for a set of sites. Section TEH1 can thus be used as an excellent example to record the regional sand dune evolution and the corresponding palaeoclimate variations in the Bayanbulak Basin. Based on these interpretations, the studied section records a dry climate between *c*. 9 and 8 kyr, a short period falling during the early Holocene if we take into account the uncertainty of the three luminescence ages determined for U1. Considering that the dated dune sand (U1) is just the crest layer of the whole dune body according to field geomorphological observation, we believe that this dry period causing sand dune accumulation might have occurred earlier than *c*. 9–8 kyr, probably during the early Holocene (e.g. 11–8 kyr). This dry event was followed by development of a weak sandy soil (U2), suggesting that effective moisture started to increase at ~7.4 kyr. In contrast to the evidence for dry condition and aeolian sand accumulation in the early Holocene, there had been no sand dune deposition after ~7.4 kyr, that is, during the middle and late Holocene. The wettest climate appears at the time between ~4.6 and 1.7 kyr, revealed by the formation of a dark soil (U3) showing strong

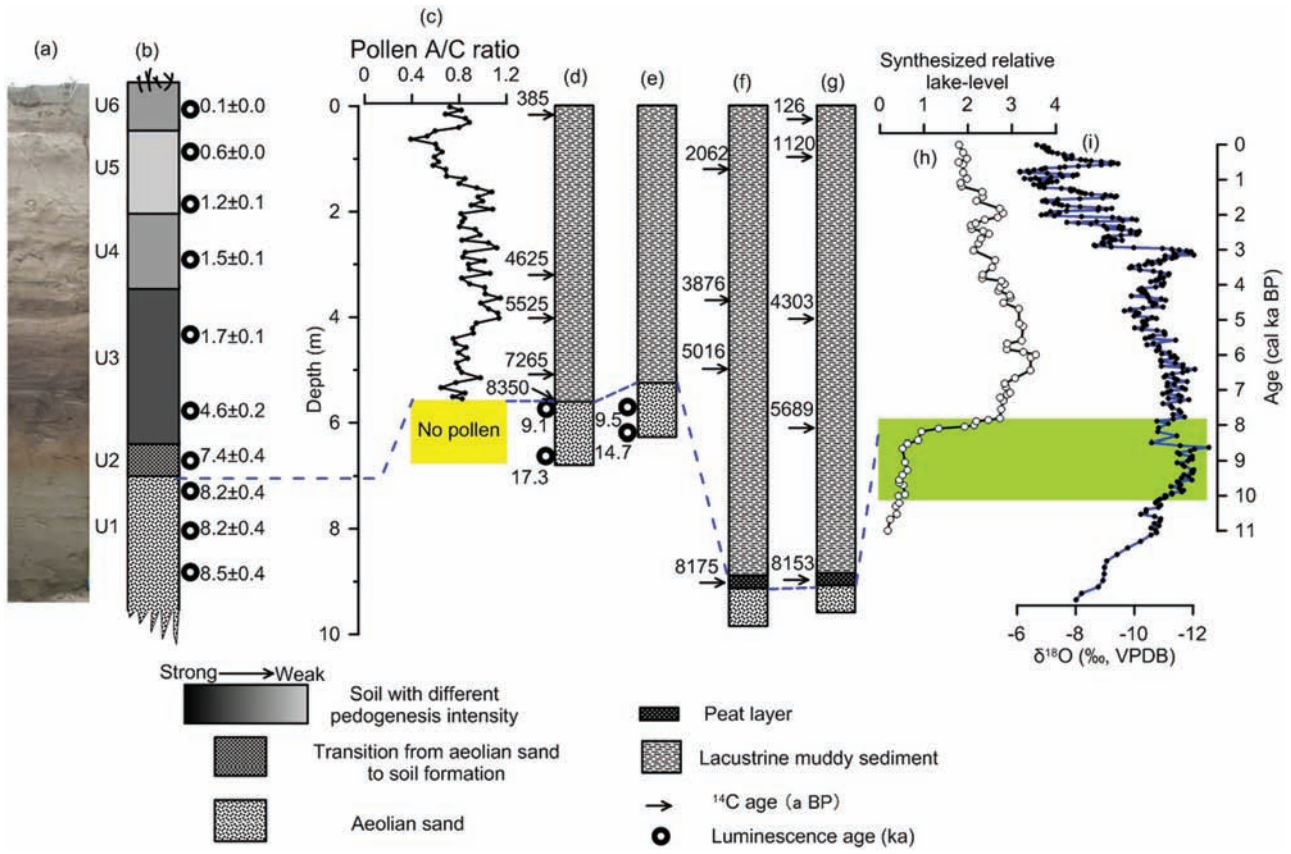

Figure 7. (a) Photo and (b) simplified stratigraphy of the TEH1 section; (d, e, f and g) show the stratigraphy and chronology of four cores (against core depth) drilled from Bosten Lake, and (c) pollen analysis (against core depth) of core d (Chen et al., 2006; Huang et al., 2009; Wünnemann et al., 2003, 2006); (h and i) denote the synthesized lake-level variation during the Holocene in the SCA (Chen et al., 2008) and the stalagmite $\delta^{18}O$ records from caves Kesang (Cheng et al., 2012), respectively. Yellowish shadow denotes the stratum without pollen in core d, and green shadow suggests significant disagreement on the moisture condition during the early Holocene derived from curves h and i. A/C: Artemisia/Chenopodiaceae; TEH1: Tianehu1; SCA: semiarid–arid Central Asia.

pedogenesis. Effective moisture seems to decrease from around 1.5 kyr to the recent but has been higher than that during the early Holocene, as evidenced by soil unit U4 with relatively weak pedogenic intensity, loess unit U5 and surface soil unit U6.

In summary, on the basis of the chronostratigraphy of section TEH1, the Holocene effective moisture variations from Bayanbulak Basin can broadly be divided into two stages, that is, a dry early Holocene, including sparse vegetation and dune mobility, and a wet middle to late Holocene, especially the wettest period between ~4.6 and 1.7 kyr.

Comparison with other palaeoclimatic records in the SCA

Many palaeoclimate records have been obtained recently from the SCA. Most of them were derived from lake sedimentary archives, which showed significant variations in lake level and the resultant effective moisture during the Holocene (e.g. Chen et al., 2008; Feng et al., 2006; Herzschuh, 2006). Nevertheless, the timing, amplitude and forcing mechanisms of palaeoclimate change (e.g. moisture variability) are 'hotly' debated. With a robust chronology and clear climatic implications, aeolian records are likely to be suitable to validate the lake records. The comparison of their palaeoclimate implications with those from lacustrine deposits could help us obtain more reliable reconstruction of past climatic change (Lu et al., 2010).

We compared the results of this study in Bayanbulak Basin (upper Kaidu River) with the nearby lake sediment–based reconstructions from Bosten Lake (mainly fed by Kaidu River; see Figure 1b for its location; Chen et al., 2006; Huang et al., 2009), which demonstrates good agreement within dating errors. As shown in Figure 7d–g, stratigraphical and chronological investigations based on luminescence and ^{14}C dating of terrestrial organic remains for four sediment cores from Bosten Lake show that the whole Bosten Lake basin dried up and was covered by aeolian sand during the late-glacial and about 8.4 cal. kyr BP (Figure 7d and e). Then, a layer of dark peat formed around 8.2 cal. kyr BP in a shallow area (Figure 7f and g; Wünnemann et al., 2003, 2006), and after 8 cal. kyr BP, a stable lake formed in this basin. Chen et al. (2006) and Huang et al. (2009) thus proposed a dry regional climate during the late-glacial and the early Holocene (16–8 cal. kyr BP), which is consistent with our palaeoclimatic data in terms of sand dune accumulation before ~8 kyr from Bayanbulak Basin. Although the climate became humid after 8 kyr in Bosten Lake, pollen Artemisia/Chenopodiaceae (A/C) ratio (Figure 7c) indicates that the climate was relatively dry between 8 and 6 kyr, while afterwards more humid conditions (~6–1.5 kyr) are assumed (Chen et al., 2006; Huang et al., 2009). This moisture pattern since 8 kyr also supports our evidence about a wet climate between ~4.6 and 1.6 kyr, as evidenced by the buried soil formation. Although there is an absence of luminescence ages for the time period between ~7.5 and 5 kyr in the section under study, we believe that this status might be consistent with relatively wet climate at that time interval, assuming that the absence of ages reflects dune stability under vegetation cover.

Furthermore, the dry climatic event before ~8 kyr, deduced from Bayanbulak Basin and Bosten Lake, occurred not only in the Kaidu River drainage, but widespreadly showed up in most

areas of the SCA as evidenced by more recent pedostratigraphies, pollen and diatom assemblages, sedimentology, lake-level variations and geochemistry (see reviews by Chen et al., 2008; Feng et al., 2006; Herzschuh, 2006). For instance, by synthesis of a set of lake records with reliable chronologies and robust proxies, Chen et al. (2008) concluded that the SCA as a whole experienced a synchronous dry climate in the early Holocene in contrast to the middle and late Holocene, inferred from the compiled Holocene lake-level variations (Figure 7h); they chose the lakes basically covering the Westerlies-dominated region of the SCA, a region extending from the Caspian Sea in the west to the modern Asian summer monsoon boundary in the east, encompassing the Central Asian countries, NW China and the southern Mongolian Plateau. Recently, using a series of simulations, Jin et al. (2012) validated this dry climate event during the early Holocene (11–8 kyr) in mid-latitude SCA.

However, it is noted that our hypothesis of the dry early Holocene seems a challenge of a new stalagmite $\delta^{18}O$ record from Kesang Cave (Cheng et al., 2012) in the middle Tien Shan Mountains of Xinjiang (see Figure 1b for its location). Based on this high-resolution and numerically dated speleothem $\delta^{18}O$ record, Cheng et al. (2012) presented a similar precipitation variability in SCA (Figure 7i) to that in monsoonal Asia during the Holocene (Fleitmann et al., 2003; Wang et al., 2008). They thus suggested incursions of Asian summer monsoon rainfall into the Tien Shan Mountains, currently controlled by Westerlies, which led to increased humidity during the early Holocene. Obviously, for the early Holocene, the increased precipitation record in the Kesang Cave area is in contrast to the reinforced aridity in Bayanbulak Basin. Nevertheless, it is possible that stalagmite $\delta^{18}O$ values are not only controlled by simple wet–dry alternations in climate. For instance, the stalagmite $\delta^{18}O$ is newly interpreted as a proxy indicator of a vapour source or track, rather than of monsoon precipitation (Maher and Thompson, 2012; Pausata et al., 2011; Tan, 2014). In addition, a widespread dry climate before ~8 kyr in the SCA, referred from both proxy records (e.g. this study and Chen et al., 2008) and modelling work (e.g. Jin et al., 2012), seems to cast doubt on the interpretation that Asian monsoon could reach the Tien Shan area during the early Holocene.

Conclusion

This study reported the aeolian record in Bayanbulak Basin to reveal regional wet/dry variations in the SCA during the Holocene. Combining luminescence dating technique and stratigraphic investigations on a sand dune/palaeosol sequence, we conclude that there was a dry climate with sand dune accumulation before ~8 kyr, and a wet phase characterized by palaeosol formation between 4.6 and 1.7 kyr. This moisture variation pattern was confirmed by nearby lacustrine sedimentary records from Bosten Lake (Chen et al., 2006; Huang et al., 2009; Wünnemann et al., 2003, 2006). Especially, the drought condition deduced from aeolian sand formation is consistent with the widespread low lake levels in most areas of the SCA during the early Holocene. Our inference is obviously inconsistent with humid early Holocene recorded by a new stalagmite $\delta^{18}O$ sequence from Kesang Cave, which is about 300 km to the west of the study area. This disagreement is likely to give rise to a challenge of the interpretation that $\delta^{18}O$ values of speleothem from the SCA are mainly controlled by Asian monsoon precipitation.

Acknowledgements

This manuscript benefited from constructive reviews from Dr Francis Mayle and two anonymous reviewers. Lei Gao is thanked for help in the field and laboratory.

Funding

This work was funded by the Natural Science Foundation (NSF) of China (grant 41271002), the Strategic Priority Research Program (Climate Change: Carbon Budget and Relevant Issues) of the Chinese Academy of Sciences (grant XDA05120102), the 'NIGLAS 1-3-5 Project' (grant NIGLAS2012135004), the Major State Basic Research Development Program of China (973 Program, 2010CB950202), the State Key Laboratory of Lake Science and Environment (grant 2012SKL002) and the Fundamental Research Funds for the Central Universities (grant lzujbky-2013-k18).

References

Aitken MJ (1985) *Thermoluminescence Dating*. London: Academic Press.

Aitken MJ (1998) *An Introduction to Optical Dating*. Oxford: Oxford University Press.

An ZS, Porter SC, Kutzbach JE et al. (2000) Asynchronous Holocene optimum of the East Asian monsoon. *Quaternary Science Reviews* 19: 743–762.

Auclair M, Lamothe M and Huot S (2003) Measurement of anomalous fading for feldspar IRSL using SAR. *Radiation Measurements* 37: 487–492.

Balescu S and Lamothe M (1994) Comparison of TL and IRSL age estimates of feldspar coarse grains from waterlain sediments. *Quaternary Science Reviews* 13: 437–444.

Bristow CS, Duller GAT and Lancaster N (2007) Age and dynamics of linear dunes in the Namib Desert. *Geology* 35: 555–558.

Broccoli AJ and Manabe S (1992) The effects of orography on midlatitude northern hemisphere dry climates. *Journal of Climate* 5: 1181–1201.

Buylaert JP, Huot S, Murray AS et al. (2011) Infrared stimulated luminescence dating of an Eemian (MIS 5e) site in Denmark using K-feldspar. *Boreas* 40: 46–56.

Buylaert JP, Jain M, Murray AS et al. (2012) A robust feldspar luminescence dating method for Middle and Late Pleistocene sediments. *Boreas* 41: 435–451.

Buylaert JP, Murray AS, Thomsen KJ et al. (2009) Testing the potential of an elevated temperature IRSL signal from K-feldspar. *Radiation Measurements* 44: 560–565.

Chase B (2009) Evaluating the use of dune sediments as a proxy for palaeo-aridity: A southern African case study. *Earth-Science Reviews* 93: 31–45.

Chase BM and Thomas DSG (2007) Multiphase late Quaternary aeolian sediment accumulation in western South Africa: Timing and relationship to palaeoclimatic changes inferred from the marine record. *Quaternary International* 166: 29–41.

Chen FH, Huang XZ, Yang ML et al. (2006) Westerly dominated Holocene climate model in arid central Asia: Case study on Bosten Lake, Xinjiang, China. *Quaternary Sciences* 26: 881–887 (in Chinese with English abstract).

Chen FH, Yu ZC, Yang ML et al. (2008) Holocene moisture evolution in arid central Asia and its out-of-phase relationship with Asian monsoon history. *Quaternary Science Reviews* 27: 351–364.

Cheng H, Zhang PZ, Spötl C et al. (2012) The climatic cyclicity in semiarid-arid central Asia over the past 500,000 years. *Geophysical Research Letters* 39: L01705. DOI: 10.1029/2011GL050202.

Dando WA (2005) Asia: Climates of Siberia, central and east Asia. In: Oliver JE (ed.) *Encyclopedia of World Climatology*. Dordrecht: Springer, pp. 102–114.

Duller GAT (1994) Luminescence dating using feldspars: A test case from southern North Island, New Zealand. *Quaternary Science Reviews* 13: 423–427.

Duller GAT (2008) Single-grain optical dating of Quaternary sediments: Why aliquot size matters in luminescence dating. *Boreas* 37: 589–612.

Feng ZD, An CB and Wang HB (2006) Holocene climatic and environmental changes in the arid and semi-arid areas of China: A review. *The Holocene* 16: 119–130.

Fleitmann D, Burns SJ, Mudelsee M et al. (2003) Holocene Forcing of the Indian Monsoon recorded in a stalagmite from Southern Oman. *Science* 300: 1737–1739.

Forman SL, Marin L, Pierson J et al. (2005) Aeolian sand depositional records from western Nebraska: Landscape response to droughts in the past 1500 years. *The Holocene* 15: 973–981.

Galbraith RF, Roberts RG, Laslett GM et al. (1999) Optical dating of single and multiple grains of quartz from Jinmium rock shelter, northern Australia: Part 1, experimental details and statistical models. *Archaeometry* 41: 339–364.

Goble RJ, Mason JA, Loope DB et al. (2004) Optical and radiocarbon ages of stacked paleosols and dune sands in the Nebraska Sand Hills, USA. *Quaternary Science Reviews* 23: 1173–1182.

Godfrey-Smith DI, Huntley DJ and Chen WH (1988) The optical behaviour of quartz and feldspar sediment extracts. *Quaternary Science Reviews* 7: 373–380.

Guérin G, Mercier N and Adamiec G (2011) Dose-rate conversion factors: Update. *Ancient TL* 29: 5–8.

Herzschuh U (2006) Palaeo-moisture evolution in monsoonal Central Asia during the last 50,000 years. *Quaternary Science Reviews* 25: 163–178.

Hou J, D'Andrea WJ and Liu Z (2012) The influence of ^{14}C reservoir age on interpretation of paleolimnological records from the Tibetan Plateau. *Quaternary Science Reviews* 48: 67–79.

Huang XZ, Chen FH, Fan YX et al. (2009) Dry late-glacial and early Holocene climate in arid central Asia indicated by lithological and palynological evidence from Bosten Lake, China. *Quaternary International* 194: 19–27.

Huntley DJ and Baril MR (1997) The K content of the K-feldspars being measured in optical dating or in thermoluminescence dating. *Ancient TL* 15: 11–13.

Huntley DJ and Hancock RGV (2001) The Rb contents of the K-feldspars being measured in optical dating. *Ancient TL* 19: 43–46.

Huntley DJ and Lamothe M (2001) Ubiquity of anomalous fading in K-feldspars and the measurement and correction for it in optical dating. *Canadian Journal of Earth Sciences* 38: 1093–1106.

Jin L, Chen F, Morrill C et al. (2012) Causes of early Holocene desertification in arid central Asia. *Climate Dynamics* 38: 1577–1591.

Lancaster N (2008) Desert dune dynamics and development: Insights from luminescence dating. *Boreas* 37: 559–573.

Li S and Fan A (2011) OSL chronology of sand deposits and climate change of last 18 ka in Gurbantunggut Desert, northwest China. *Journal of Quaternary Science* 26: 813–818.

Li B, Li SH, Wintle AG et al. (2008) Isochron dating of sediments using luminescence of K-feldspar grains. *Journal of Geophysical Research* 113: F02026. DOI: 10.1029/2007JF000900.

Li GQ, Zhao H and Chen FH (2011a) Comparison of three K-feldspar luminescence dating methods for Holocene samples. *Geochronometria* 38: 14–22.

Li X, Zhao K, Dodson J et al. (2011b) Moisture dynamics in central Asia for the last 15 kyr: New evidence from Yili Valley, Xinjiang, NW China. *Quaternary Science Reviews* 30: 3457–3466.

Long H, Lai Z, Frenzel P et al. (2012a) Holocene moist period recorded by the chronostratigraphy of a lake sedimentary sequence from Lake Tangra Yumco on the south Tibetan Plateau. *Quaternary Geochronology* 10: 136–142.

Long H, Lai Z, Fuchs M et al. (2012b) Palaeodunes intercalated in loess strata from the western Chinese Loess Plateau: Timing and palaeoclimatic implications. *Quaternary International* 263: 37–45.

Long H, Lai Z, Fuchs M et al. (2012c) Timing of Late Quaternary palaeolake evolution in Tengger Desert of northern China and its possible forcing mechanisms. *Global and Planetary Change* 92–93: 119–129.

Long H, Lai Z, Wang N et al. (2010) Holocene climate variations from Zhuyeze terminal lake records in East Asian monsoon margin in arid northern China: A multi-proxy and geomorphological study. *Quaternary Research* 74: 46–56.

Long H, Lai Z, Wang N et al. (2011) A combined luminescence and radiocarbon dating study of Holocene lacustrine sediments from arid northern China. *Quaternary Geochronology* 6: 1–9.

Lu H, Mason J, Stevens T et al. (2011) Response of surface processes to climatic change in the dunefields and Loess Plateau of North China during the late Quaternary. *Earth Surface Processes and Landforms* 36: 1590–1603.

Lu H, Miao X, Zhou Y et al. (2005) Late Quaternary aeolian activity in the Mu Us and Otindag dune fields (north China) and lagged response to insolation forcing. *Geophysical Research Letters* 32: L21716. DOI: 10.1029/2005GL024560.

Lu H, Zhao C, Mason J et al. (2010) Holocene climatic changes revealed by aeolian deposits from the Qinghai Lakearea (northeastern Qinghai-Tibetan Plateau) and possible forcing mechanisms. *The Holocene* 21(2): 297–304.

Madsen AT, Buylaert JP and Murray AS (2011) Luminescence dating of young coastal deposits from New Zealand using feldspar. *Geochronometria* 38: 378–390.

Maher BA and Thompson R (2012) Oxygen isotopes from Chinese caves: Records not of monsoon rainfall but of circulation regime. *Journal of Quaternary Science* 27: 615–624.

Mason JA, Lu H, Zhou Y et al. (2009) Dune mobility and aridity at the desert margin of northern China at a time of peak monsoon strength. *Geology* 37: 947–950.

Mason JA, Swinehart JB, Goble RJ et al. (2004) Late Holocene dune activity linked to hydrological drought, Nebraska Sand Hills, USA. *The Holocene* 14: 209–217.

Mejdahl V (1979) Thermoluminescence dating: Beta attenuation in quartz grains. *Archaeometry* 21: 61–73.

Miao X, Mason JA, Swinehart JB et al. (2007) A 10,000 year record of dune activity, dust storms, and severe drought in the central Great Plains. *Geology* 35: 119–122.

Mischke S, Weynell M, Zhang C et al. (2013) Spatial variability of ^{14}C reservoir effects in Tibetan Plateau lakes. *Quaternary International* 313–314: 147–155.

Pausata FSR, Battisti DS, Nisancioglu KH et al. (2011) Chinese stalagmite $\delta^{18}O$ controlled by changes in the Indian monsoon during a simulated Heinrich event. *Nature Geoscience* 4: 474–480.

Prescott JR and Hutton JT (1994) Cosmic ray distributions to dose rates for luminescence and ESR dating: Large depths and long-term variations. *Radiation Measurements* 23: 497–500.

Reimann T and Tsukamoto S (2012) Dating the recent past (<500 years) by post-IR IRSL feldspar – Examples from the North Sea and Baltic Sea coast. *Quaternary Geochronology* 10: 180–187.

Reimann T, Tsukamoto S, Naumann M et al. (2011) The potential of using K-rich feldspars for optical dating of young coastal sediments – A test case from Darsse Zingst peninsula (southern Baltic Sea coast). *Quaternary Geochronology* 6: 207–222.

Singhvi AK and Porat N (2008) Impact of luminescence dating on geomorphological palaeoclimate research in drylands. *Boreas* 37: 536–558.

Tan M (2014) Circulation effect: Response of precipitation $\delta^{18}O$ to the ENSO cycle in monsoon regions of China. *Climate Dynamics* 42: 1067–1077.

Telfer MW and Thomas DSG (2007) Late Quaternary linear dune accumulation and chronostratigraphy of the southwestern Kalahari: Implications for aeolian palaeoclimatic reconstructions and predictions of future dynamics. *Quaternary Science Reviews* 26: 2617–2630.

Thiel C, Buylaert JP, Murray AS et al. (2011) Luminescence dating of the Stratzing loess profile (Austria) – Testing the potential of an elevated temperature post-IR IRSL protocol. *Quaternary International* 234: 23–31.

Thomas DSG and Burrough SL (2012) Interpreting geoproxies of late Quaternary climate in African drylands: Implications for understanding environmental change and early human behavior. *Quaternary International* 253: 5–17.

Thomsen KJ, Murray AS, Jain M et al. (2008) Laboratory fading rates of various luminescence signals from feldspar-rich sediment extracts. *Radiation Measurements* 43: 1474–1486.

Wallinga J, Bos AJJ, Dorenbos P et al. (2007) A test case for anomalous fading correction in IRSL dating. *Quaternary Geochronology* 2: 216–221.

Wang YJ, Cheng H, Edwards RL et al. (2005) The Holocene Asian Monsoon: Links to solar changes and North Atlantic Climate. *Science* 308: 854–857.

Wang Y, Liu X and Herzschuh U (2010) Asynchronous evolution of the Indian and East Asian Summer Monsoon indicated by Holocene moisture patterns in monsoonal central Asia. *Earth-Science Reviews* 103: 135–153.

Wintle AG (1973) Anomalous fading of thermoluminescence in mineral samples. *Nature* 245: 143–144.

Wünnemann B, Chen FH, Riedel F et al. (2003) Holocene lake deposits of Bosten Lake, southern Xinjiang, China. *Chinese Science Bulletin* 48: 1429–1432.

Wünnemann B, Mischke S and Chen FH (2006) A Holocene sedimentary record from Bosten Lake, China. *Palaeogeography, Palaeoclimatology, Palaeoecology* 234: 223–238.

Yang L, Wang T, Zhou J et al. (2012) OSL chronology and possible forcing mechanisms of dune evolution in the Horqin dunefield in northern China since the Last Glacial Maximum. *Quaternary Research* 78: 185–196.

Yang X, Wang X, Liu Z et al. (2013) Initiation and variation of the dune fields in semi-arid China – with a special reference to the Hunshandake Sandy Land, Inner Mongolia. *Quaternary Science Reviews* 50: 369–380.